

Efficient Multi-user Offloading of Personalized Diffusion Models: A DRL-Convex Hybrid Solution

Wanting Yang, Zehui Xiong, *Senior Member, IEEE*, Song Guo, *Fellow, IEEE*,
Shiwen Mao, *Fellow, IEEE*, Dong In Kim, *Fellow, IEEE*, Merouane Debbah *Fellow, IEEE*

Abstract—With the impressive generative capabilities of diffusion models, personalized content synthesis has emerged as the most highly anticipated. However, the large model sizes and iterative nature of inference make it difficult to deploy personalized diffusion models broadly on local devices with varying computational power. To this end, we propose a novel framework for efficient multi-user offloading of personalized diffusion models, given a variable number of users, diverse user computational capabilities, and fluctuating available computational resources on the edge server. To enhance computational efficiency and reduce storage burden on edge servers, we first propose a tailored multi-user hybrid inference manner, where the inference process for each user is split into two phases with an optimizable split point. The initial phase of inference is processed on a cluster-wide model using batching techniques, generating low-level semantic information corresponding to each user’s prompt. Then, the users employ their own personalized model to add further details in the later inference phase. Given the constraints on edge server computational resources and users’ preferences for low latency and high accuracy, we model the joint optimization of each user’s offloading request handling and split point as an extension of the Generalized Quadratic Assignment Problem (GQAP). Our objective is to maximize a comprehensive metric that accounts for both latency and accuracy across all users. To tackle this NP-hard problem, we transform the GQAP into an adaptive decision sequence, model it as a Markov decision process, and develop a hybrid solution combining deep reinforcement learning with convex optimization techniques. Simulation results validate the effectiveness of our framework, demonstrating superior optimality and low complexity compared to traditional methods.

Index Terms—Diffusion model, edge offloading, generalized quadratic assignment problem, DRL, AIGC service, hybrid inference

arXiv:2411.15781v1 [cs.LG] 24 Nov 2024

1 INTRODUCTION

The remarkable progress of generative models has ushered in a new era of artificial intelligence technology. Notable advancements, such as ChatGPT in natural language processing, have demonstrated capabilities on par with human experts across a wide range of applications. Similarly, Stable Diffusion Models (SDMs) [1], developed based on Denoising Diffusion Probabilistic Models [2], has also achieved comparable prominence in computer vision. The impressive generative capabilities of SDMs have established them as a foundational tool in numerous applications, including *super-resolution*, *image editing*, *text-to-image* and *inpainting*, etc. [3], as well as *semantic decoding* in semantic communication [4]. Among these advanced applications, personalized content synthesis (PCS) stands out as one of the most important and eagerly anticipated branches of research.

The customizable features of PCS for objects, styles, faces, and other high-level semantic information allow users

to generate images of themselves in various settings or recreate rare behaviors of their pets. This capability has driven growing public interest, prompting numerous researchers and companies to focus on this specific generation task. Since the release of *DreamBooth* and *Textual Inversion* in August 2022, over 100 methods have emerged in this field within a remarkably short period [5]. Meanwhile, rising privacy concerns associated with PCS, coupled with a growing number of daily active users, have created a strong demand for on-device SDMs. However, these models often come with large model sizes and significant computational overhead. In this sense, given slow and iterative sampling process during inference, the practical application of personalized SDMs remains constrained by the diverse computational capabilities of user devices.

Recently, research aimed at addressing the above issues can be categorized into the following three areas. The first focuses on *sampling step reduction*, which is best known for its implementation in Denoising diffusion implicit models (DDIMs) [6]. However, it is important to note that a lower number of denoising steps implies reduced detail generation capability and less stability in the quality of the generated images. The second approach involves *model compression*, including architecture redesign [7], network pruning [8], and quantization [9]. Despite these efforts, achieving semantic consistency comparable to larger models remains challenging. The third category, *hybrid inference*, includes (1) combining models of different sizes to offset quality degradation from exclusive reliance on compressed models [10], and (2) leveraging edge server’s greater computing power

Manuscript received ...

Wanting Yang and Zehui Xiong are with the Pillar of Information Systems Technology and Design, Singapore University of Technology and Design, Singapore (e-mail: wanting_yang@sutd.edu.sg; zehui_xiong@sutd.edu.sg); Song Guo is with the Department of Computer Science and Engineering, The Hong Kong University of Science and Technology, Hong Kong, SAR, China (e-mail: songguo@cse.ust.hk); Shiwen Mao is with the Department of Electrical and Computer Engineering, Auburn University, Auburn 36830, USA (e-mail: smao@ieee.org); Dong In Kim is with the Department of Electrical and Computer Engineering, Sungkyunkwan University, Suwon 16419, South Korea (e-mail: dongin@skku.edu); Merouane Debbah is with KU 6G Research Center, Khalifa University of Science and Technology, P O Box 127788, Abu Dhabi, UAE (email: merouane.debbah@ku.ac.ae) and also with CentraleSupélec, University Paris-Saclay, 91192 Gif-sur-Yvette, France.

to offload part of the denoising steps, enabling collaborative inference and reducing overall latency [11].

Among the above discussed approaches, the DDIM has been integrated into SDMs. However, generating high-quality and detail-rich images still requires hundreds of denoising steps, which is still constrained by the limited computational power of local devices, which restricts the broader on-device SDMs. In recent work [12], *ByteDance Inc.* combines the aforementioned model compression and both hybrid inference methods for SDMs. The inference process begins with a smaller model on the user side, while the latter denoising steps, which require additional detail, are completed by a large-scale model on the cloud. The simulation results confirm the promising gains brought by this *composite hybrid inference* approach. However, if extended to a more practical multi-user scenario with personalized SDMs, the differentiated, personalized models for each user would impose significant storage and computational burdens on the cloud, deviating from the trend toward on-device applications. *To address the strong demand for multi-user personalized SDMs and bridge gaps in current research, this work focuses on practical implementations.*

Extending beyond specific optimizations of inference algorithms, our goal is to seamlessly integrate inference optimization with real-world resource management under the typical edge-device collaborative architecture of future networks. While edge-assisted offloading and inference have been explored for some time, new challenges emerge that the larger model size and iterative sampling nature of SDMs render existing offloading methods ineffective. Large deep neural networks (DNNs) are typically partitioned to offload portions to the edge, thereby reducing storage and computational demands on local devices. However, partitioning the backbone of SDMs across the local devices and edge server introduces excessive communication overhead due to the iterative sampling process. Thus, offloading for SDMs must focus on optimizing the number of denoising steps offloaded, which requires the edge server to host a complete backbone model. Unlike the shared foundation models, personalized requirements mean that each user’s diffusion model is unique. Duplicating each personalized model on the edge server for independent inference would demand immense storage and computational resources, potentially exceeding even the capabilities of cloud infrastructure.

To overcome this dilemma and facilitate the widespread adoption of personalized SDMs, we propose a novel framework for efficient multi-user offloading of personalized diffusion models. This framework is designed for a highly practical scenario that includes a variable number of users, diverse user computational capabilities, and fluctuating available computational resources on the edge server. Specifically, to reduce redundancy in model deployment and alleviate storage burdens on the edge server, we introduce a cluster-wide model as a shared offloading model across multiple users. To further enhance computational efficiency, we assume that the offloading tasks of multiple users can be processed in batches. However, these two improvements also introduce two new issues.

- The hybrid inference approach, which combines the offloaded inference by the cluster-wide model with local inference by the personalized model, introduces a de-

gree of personalization loss. As a result, while offloading reduces inference latency, it also decreases the accuracy of personalized feature representation. Thus, a trade-off between latency reduction and preservation of personalization must be carefully considered when optimizing offloading steps.

- In the batching technique, an increase in batch size causes the inference latency for each denoising step to grow, thereby intensifies the interdependence between each user’s offloading decision and the overall system performance. Unlike existing works that ignore the parallel inference capability of the server and assume that the total latency of multiple tasks is proportional to the total number of tasks, our optimization objective is formulated as a quadratic function of the decision variables.

To resolve the above issues, we innovatively establish a comprehensive and precise optimization metric and newly design a low-complexity solution for extended Generalized Quadratic Assignment Problem (GQAP). In this work, we focus on a cluster within the same geographic region, utilizing similar personalized generative applications as the basis of our exploration. The specific contributions are summarized as follows:

- We propose an efficient multi-user hybrid inference manner. In this framework, a cluster-wide SDMs, which is trained to capture common features of personalized demands among users within the cluster, is located at the edge server. Meanwhile, the personalized model of each user is deployed at the local individually. The inference process for each user is split into two phases with an *optimizable split point*. For users participating in offloading, the initial phase of inference is performed on the cluster-wide model using batching techniques. This approach synchronously generates low-level semantic and contour information tailored to each user’s prompt. The intermediate results are subsequently returned to each user, who then applies a personalized SDM to add finer details in the later stages of the generation process.
- We propose a tailored metric that balances latency and accuracy of personalized feature, interconnected through a weighting parameter. This parameter captures each user’s preference between the two factors and can be customized individually to reflect their specific requirements. Based on rigorous mathematical analysis, we provide the range for this parameter along with insights into the corresponding effects. To quantify accuracy in PCS, we define a metric called Personalized Accuracy Index (PAI), which jointly considers the traditional accuracy, measured by the CLIP, and the variation in final generated images for different users given the same prompt, assessed by LPIPS. We train a cluster-wide model and multiple personalized models using DreamBooth and establish a unified mathematical model describing the relationship between PAI and the split point based on empirical simulations.
- We formulate the joint optimization of offloading request handling and each user’s individual split point as an extended GQAP, aiming to maximize overall performance using the tailored metric as a guiding principle. To meet the real-time decision-making requirements, we are, to the best of our knowledge, the first to apply Deep Re-

inforcement Learning (DRL) to solve GQAP, proposing a DRL-convex hybrid solution. Specifically, we introduce a novel paradigm that transforms GQAP into a sequential decision-making process and maps it into a Markov Decision Process (MDP) model. Meanwhile, we determine the optimal split point for each user based on convex optimization theory and integrate it into the environment of the MDP. We compare this algorithm with classical algorithms for solving GQAP, such as Branch & Bound and heuristic algorithms, demonstrating its optimality and low complexity, $O(n)$, regarding the number of users.

The rest of this paper is organized as follows. In Section 2, we review research in hybrid inference for SDMs and the existing solutions relevant to GQAP. Then, in Section 3, we introduce the system overview, and relevant models. Then, we present the problem formulation in Section 4 and the DRL-convex hybrid solution is described in Section 5. An experimental evaluation is presented in Section 6, followed by the conclusion and future directions in Section 7.

2 RELATED WORKS

2.1 Hybrid Inference for Diffusion Models

Since the remarkable success of diffusion models in generative tasks, research on latency optimization in their inference processes has gained momentum. As discussed in Section I, this research initially focused on reducing denoising steps and compressing the model. However, both approaches inevitably lead to some degree of performance degradation; the greater the reduction in inference latency, the more noticeable the performance loss. Beyond these two approaches, hybrid inference has been proposed, offering flexible combinations with the above methods.

In 2022, NVIDIA Corporation first proposed the eDiff-I framework, where the inference process is divided into multiple stages. Each stage corresponds to a distinct model, focusing on different generative functions to enhance overall inference performance [13]. Then, the authors in [14] design OMS-DPM, a predictor-based search algorithm, to determine the optimal model schedule given a specific generation time budget and a set of pre-trained models. Recently, in [15], the authors present a new framework called DDSM, which employs a spectrum of neural networks whose sizes are adapted according to the importance of each generative step. In addition to the model’s size and functionality, the authors in [16] expand the concept of hybrid inference to incorporate computational heterogeneity within the inference process. Here, the inference process is split, with one part completed by a more powerful edge server and the latter part handled locally by the user device, connected via a wireless transmission link to reduce inference latency. Additionally, they propose an interesting idea: users with similar prompts can share the initial portion of the inference process on the edge server, reducing the edge server’s computational load. However, this inevitably comes at the cost of lower image generation quality. To address this, the authors in [17] further optimize the split point under this setting. Although the framework’s effectiveness is applicable when prompts from different users are highly similar, in practice, user prompts are often diverse. Therefore, this framework’s use cases are quite limited.

In addition, ByteDance further extends hybrid inference to simultaneously incorporate both model heterogeneity and computational heterogeneity, as introduced in the *Introduction* [12]. However, they only consider the single-user inference scenario and do not address the inevitable challenges in real-world applications, where cloud server resources available to users are limited. Consequently, they do not explore the necessary handling of offloading requests or the optimization of the split point based on personalized user requirements under such conditions. Overall, optimization of diffusion model inference for real-world applications remains in a very early stage.

2.2 Generalized Quadratic Assignment Problem

Combinatorial optimization problems (COPs) are widely present in network resource optimization, including the *traveling salesman problem* [18], *knapsack problem* [19], and *multi-armed bandit problem* [20], etc. Among them, quadratic assignment problem (QAP) is considered as one of the most difficult to solve in combinatorial optimization [21]. In addition, various variants of this problem, such as *Quadratic Bottleneck Assignment Problem*, *Biquadratic QAP*, *quadratic semi-assignment problem* and the relatively new *GQAP*, have continuously emerged, attracting significant attention over the past decades. A common approach is to linearize the quadratic terms using linearization techniques, enabling the problems to be solved with general-purpose mixed integer linear programming solvers. Two widely used techniques are standard linearization [22] and the reformulation-linearization technique (RLT) [23]. Meanwhile, the authors in [24] further integrate Lagrangean relaxation procedure over RLT, then combine with the classic Branch & Bound scheme. Nevertheless, the quadratic form of its objective function makes it challenging to find even an approximate optimal solution within limited time, especially when the problem size is slightly larger. To this end, the authors in [21] propose a heuristic algorithm, a parallel iterated tabu search algorithm. Although it outperforms traditional integer linear programming solvers in terms of performance, its high computational complexity makes it challenging to apply in real-time optimization scenarios.

Meanwhile, the success of DRL in solving increasingly complex problems over the past decade has also inspired a wave of research on using DRL to tackle COPs with low complexity. Notable achievements have been made in solving problems such as the TSP, Vehicle Routing Problem, and Maximum Cut [25]–[27]. The basic idea is to transform the optimization of a high-dimensional variable into a decision sequence, thus formulating it as an MDP model dependent on a DRL paradigm. However, unlike ordering problems such as the TSP, the QAP problem is less amenable to this type of transformation, and thus using DRL to solve QAP has received relatively little attention. To our knowledge, only two studies have explored this approach. In [28], the authors identify the challenges of generalizing existing frameworks for TSP on QAP. Moreover, in [29] the authors leverage a novel double pointer network, which alternates between selecting a location for the next facility and choosing a facility for the previously selected location. Although the effectiveness of this paradigm has been

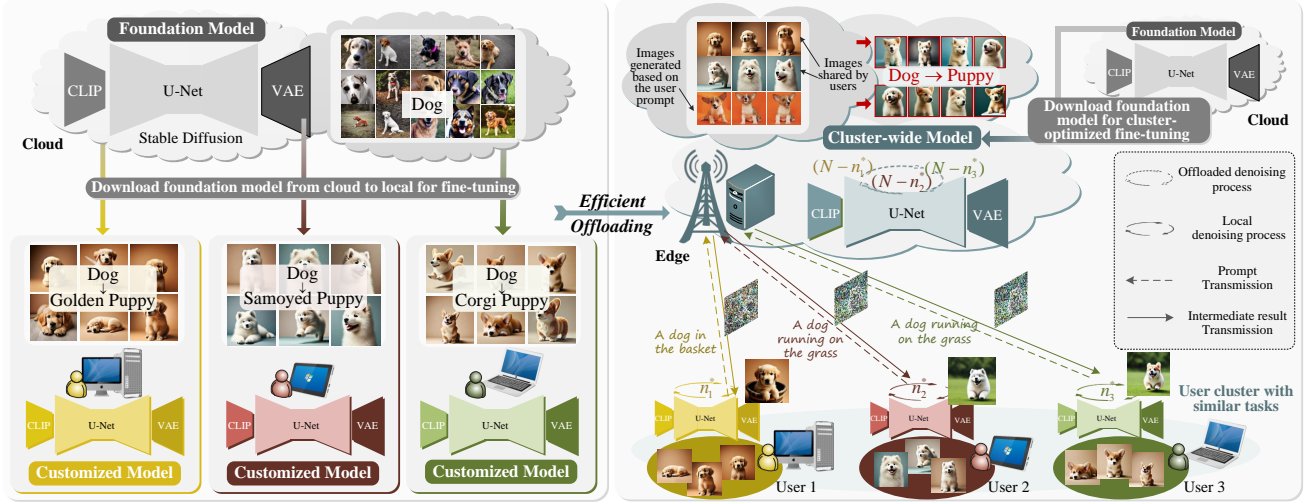


Fig. 1: Illustration of system overview and pre-deployment approach.

demonstrated, it is limited to standard QAP that requires an equal number of facilities and locations. Consequently, the algorithm's applicability is restricted. In summary, a low-complexity algorithm for addressing the GQAP remains an open research area.

3 SYSTEM MODEL AND PRE-DEPLOYMENT

3.1 System Overview

We consider a single-cell scenario with a cluster of users running the *customized* on-device applications based on SDMs. Meanwhile, for users within a cluster, we assume their PCS tasks share similarities, such as personalized dog object generation, personalized female face generation, or similar personalized style. Moreover, the devices of the users, such as desktops, laptops, and smart mobile devices, are characterized by diverse computational power. To reduce computational latency and facilitate the application proliferation, users can access edge offloading services. However, user-specific model deployment at the edge leads to considerable storage overhead. To this end, an efficient offloading manner is considered in this work. As shown in Fig. 1, these customized on-device applications are assumed to share a cluster-wide model hosted on the edge server. This model, derived through cluster-oriented fine-tuning, enables efficient parallel processing of tasks with batching techniques. A feasible pre-deployment approach is detailed in Section 3.2.

To maximize overall system efficiency and performance, we adopt a periodic & centralized offloading mechanism. We assume that the offloading strategy is executed at fixed intervals of duration Δ , each consisting of K time slots, where each time slot is indexed by k . Moreover, we denote the set of users sending requests during Δ as \mathcal{I} , with each user indexed by i . A user $i \in \mathcal{I}$ can send an offloading request at any time slot k , but must wait $(K-k)$ time slots to receive the server's feedback. This time interval is referred to as round-trip time (RTT), denoted by ℓ^R . Moreover, we denote the number of available GPUs for the current user set \mathcal{I} by G , which may vary over time. We define that the offloading decisions made by the edge server for user

requests include two options: *grant* and *deny* [19]. For the grant decision, the *number of offloaded denoising steps* is required to be identified at the same time. All the decisions for the users in \mathcal{I} are jointly determined by four main factors: 1) the computational capacity of the users' devices; 2) the preferences for personalized accuracy and latency; 3) the time of the request; and 4) the current available resources at the edge. As with any trade-off, the degree of inference offloading inversely impacts the extent of degradation in meeting users' personalized requirements. In this sense, these factors are considered to achieve a desired trade-off between latency and the final personalized accuracy for all users. The metrics about latency and personalized accuracy are specified in Section 3.4.

Once the offloading strategy is determined, all denoising steps for users who are denied are performed locally on their devices. For users who are granted, they first need to transmit their prompts to the edge server. The edge server, based on the offloading strategy results for each user, performs the user-specific number of denoising steps at the edge for each user's prompt, respectively. The intermediate results are then feedback to the users to complete the remaining offloading locally. (The hybrid inference model is detailed in Section 3.3.) For the uplink and downlink transmission involved in the process, we assume that the spectral efficiency η (or data rate per unit bandwidth) for user i is fixed, with a given modulation and coding scheme. Given that the transmission latency is remarkably lower than the computational latency, we simplify the bandwidth allocation. We assume that during the transmission process, all users granted for offloading equally share the system's reserved maximum bandwidth W_{\max} .

3.2 Pre-deployment Approach

Subsequently, we introduce a pre-deployment approach for the considered multi-user scenario as stated in Section 3.1. For illustration purposes, we consider the SDM-based on-device applications with *personalized object generation*. This approach, however, is equally applicable to personalization tasks involving facial features, style customization, etc., sup-

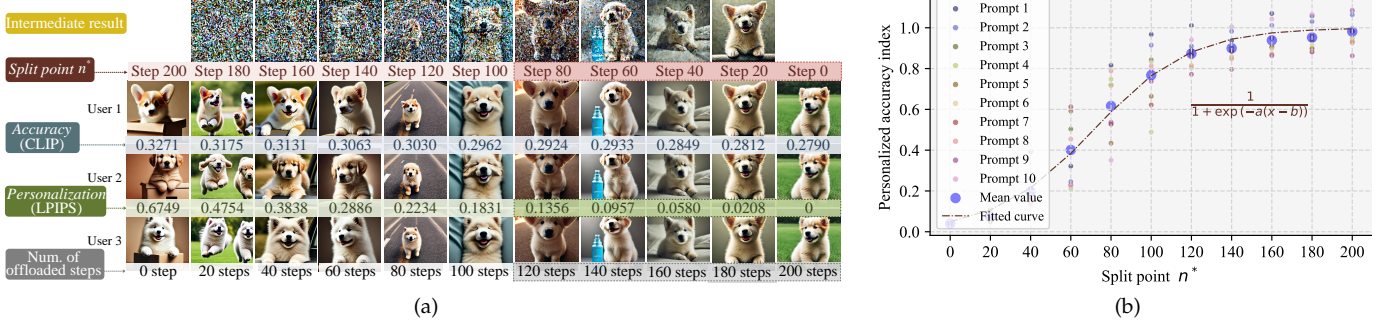


Fig. 4: Illustration of personalized accuracy metric. (a) The selected visualization results, along with the mean values of accuracy and personalization for CLIP and LPIPS metrics across 200 data sets generated from 10 different prompts at various split points; (b) The fitting curve for the relationship between PAI and the split point with $a_{\mathcal{F}} = 0.0413$ and $b_{\mathcal{F}} = 71.44$.

with the split point $n_i^* \in [\hat{N}, N]$, the denoising steps from N to $n_i^* + 1$ are executed at the edge, and the remaining denoising steps from n_i^* to 1 are performed locally. For an extreme case, $n_i^* = N$ indicates that the entire inference process is performed locally.

Moreover, as shown in the top of Fig. 2, To optimize the offloading process at the edge, the batching technique is employed to harness parallel computing capabilities and reduce memory access time. Specifically, at intervals of duration Δ , the edge server assembles the pure noisy data, denoising step indexes, and prompts of all the granted users, and batches them separately. Then, the formed three individual batches are fed as three distinct inputs into the model for parallel and iterative inference. Due to varying offloading task volumes among different users, some tasks may complete earlier, resulting in a reduced batch size. According to the NVIDIA report¹, when utilizing the batching technique, the function of the computational latency on the batch size for a specific neural network is observed to be approximately linear, usually with a large constant term [19]. In this context, we use $\mathcal{L}(b) = kb + h$ to characterize the computational latency of *one denoising step*, where b represents the batch size. Meanwhile, k and h are constant terms whose values depend on the adopted models of GPUs, which can be determined experimentally as shown in Fig. 3. Hereinafter, for the sake of simplicity, we use (k_i, h_i) and (k_e, h_e) to characterize the computation power of user i and edge server, respectively. For the local inference, we can default the value of b to always be 1. Then, we denote the latency per local denoising step for user i by $\mathcal{L}_i(1)$ for short. Furthermore, considering the commonly used data partitioning approach in parallel inference, we assume that with G GPUs on the edge server, the inference latency can be approximately reduced to the latency corresponding to a batch size of $1/G$ of the original, that is, $\mathcal{L}(b)$ can be further modified as $\mathcal{L}_e(b, G) \approx k_e(b/G) + h_e$.

3.4 Quality of Experience Metric

3.4.1 End-to-end latency

The end-to-end (E2E) latency for a stable diffusion task is measured from the moment the user sends the offloading request to the edge server until the final generated image is obtained. As stated in Section 3.1, the edge server responds to requests in two ways, each leading to a different composition of E2E latency. For users whose requests are denied, the E2E latency is equivalent to the sum of RTT and the latency of full local inference, expressed as $L_i = \ell_i^R + \ell_i^L$. For users whose requests are granted, the E2E latency includes two additional components, which is given by $L_i = \ell_i^R + \ell_i^E + \ell_i^T + \ell_i^L$, where ℓ_i^E denotes the inference latency at the edge, and ℓ_i^T represents the total transmission latency, including both uplink and downlink. The detailed E2E latency calculations under a given strategy policy are provided in Section 4.

3.4.2 Personalized accuracy index

In the context of efficient diffusion offloading, we introduce a tailored metric called the Personalized Accuracy Index (PAI), which integrates both personalization and accuracy. To optimize the offloading strategy, we establish the relation between PAI and the optimal split point n^* . Specifically, for accuracy measurement, we leverage the CLIP model to assess the traditional accuracy, that is, the similarity between the generated images and the user's prompt with personalized description added, denoted as $\text{CLIP}(p_i, m_i)$. To quantify personalized performance in hybrid inference, we use the LPIPS model to measure differences in the final images generated by individual users, which is expressed by $\overline{\text{LPIPS}} = \mathbb{E}_{1 \leq i < i' \leq |Z|} [\text{LPIPS}(m_i, m_{i'})]$. These images denoted by $m_i, m_{i'}$ are based on the same intermediate result provided by the cluster-wide model at the edge server, with each user applying their customized models for subsequent denoising inference. In this sense, a greater difference between the images generated by different users indicates stronger personalization. Moreover, from Fig. 4a, we can observe that, as the split point decreases (the number of offloading steps increases), both the accuracy and personalization metrics exhibit a downward trend, with the decline in personalization being more pronounced. However, as seen

1. <https://www.nvidia.com/content/dam/en-zz/Solutions/Data-Center/tesla-product-literature/t4-inference-print-update-inference-tech-overview-final.pdf>

from the visualized images, the personalized features of each user are still retained within the range of $n^* \in [80, 200]$. A significant drop in the accuracy of personalized features begins around $n^* \in [60, 80]$. Moreover, differences in the final images generated by individual users are becoming negligible and barely perceptible within $n^* \in [0, 60]$. In this sense, we specify \hat{N} as 80. Moreover, to capture this effect, we modulate the LPIPS values using a sigmoid function, $\sigma_P(x) = \frac{1}{1+\exp(-a(x-b))}$, where $x = \overline{\text{LPIPS}}$ with varying split point, b represents the threshold at which personalization undergoes a significant shift, and a indicates the slope of this change. Based on the range of $\overline{\text{LPIPS}}$ values and our observations, we set $a = 30$ and $b = 0.1$. Considering the interdependence and mutual reinforcement between accuracy and personalization, the PAI can be expressed by

$$\text{PAI} = \kappa \cdot \mathbb{E}_{i \in \mathcal{I}_t} [\text{CLIP}(p_i, m_i)] \cdot \sigma_P(\overline{\text{LPIPS}}), \quad (1)$$

where $\kappa = 3$. Then, we present a scatterplot depicting the mean PAI values for 20 images generated per prompt, across 10 different prompts, with varying numbers of split point n^* as shown in Fig. 4b. Similarly, we also use the sigmoid fitting approach for these scatter points, with $a_{\mathcal{F}} = 0.0413$ and $b_{\mathcal{F}} = 71.44$, which is denoted by $\mathcal{F}(\cdot)$. This function is utilized in Section 4 to formulate the objective function that guides the optimization of the offloading strategy.

4 PROBLEM FORMULATION FOR EFFICIENT EDGE-ASSISTED OFFLOADING

As stated in Section 3.3, we assume that the edge server allocates G GPUs to the set \mathcal{I} of users who have sent requests within the past time period Δ . Therefore, we assume that the current offloading will not impact the performance of previous offloading strategies, and likewise, the performance of the current offloading strategy will not be affected by subsequent offloading. In this sense, we mainly focus on one snapshot of personalized diffusion model offloading without loss of generality.

Before presenting the problem formulation, we first represent the outcome of the offloading strategy by a one-hot matrix $\mathbf{x}^{|\mathcal{I}| \times |\mathcal{D}|}$ and an integer index vector $\mathbf{n}^{*|\mathcal{I}| \times 1}$. Specifically, we define two binary decision variables, x_i^g and x_i^d , corresponding to *grant* and *deny*, respectively. For simplicity in subsequent notation, we abbreviate as x_i^j , $j \in \mathcal{D} = \{g, d\}$. If $x_i^j = 1$, it indicates that the request handling corresponding to j is selected for user i . In this sense, we should ensure

$$\text{C1: } \sum_{j \in \mathcal{D}} x_i^j = 1, \quad \forall i \in \mathcal{I}, \quad (2)$$

which signifies the condition that each request has only one handling approach. Meanwhile, considering computational and communication efficiency as well as stability, we assume that the edge server imposes a concurrent user limit for the number of users performing offloading in a single round, denoted B_{\max} . In this sense, we have a common constraint in offloading tasks, as below,

$$\text{C2: } \sum_{i \in \mathcal{I}} x_i^g \leq B_{\max}. \quad (3)$$

In addition, for the split point determined by the offloading strategy for user i , we denote it as n_i^* , which is consistent with the definition of n^* in Section 3.4. Therefore, we have

$$\text{C3: } \hat{N} \leq n_i^* \leq N, \quad \forall i \in \mathcal{I}. \quad (4)$$

Moreover, given the coupled relationship between decision variables \mathbf{x} and \mathbf{n}^* , an additional constraint is required as below,

$$\text{C4: } x_i^d \cdot (N - n_i^*) = 0, \quad \forall i \in \mathcal{I}, \quad (5)$$

which indicates that for users who do not offload, all denoising steps are completed locally, with the split point determined as $n_i^* = N$.

After defining the decision variables and their domains, we proceed to detail the objective function based on the QoE metrics defined in Section 3.4. First, we assign each user an individual weight parameter, denoted as α_i , which characterizes their emphasis on latency and PAI. The value of α_i can vary for each user. Therefore, the QoE of user i can be comprehensively evaluated as $\alpha_i \mathcal{F}(n_i^*) - L_i$. According to the definitions of the two forms of E2E latency in Section 3.4.1, by integrating the decision variables \mathbf{x} into L_i , L_i can be uniformly expressed as

$$L_i = \ell^R + \ell^T \cdot x_i^g + \ell^E \cdot x_i^g + \ell^L. \quad (6)$$

Therein, $\ell^R = K - k$, which is consistent for all users regardless of the different request handling they are assigned with. Meanwhile, ℓ^L is also a common term for the E2E latency corresponding to different request handling results, but its representation varies. For $x_i^d = 1$, the expression of ℓ^L is fixed as $\ell^L = N \mathcal{L}_i(1)$, while for $x_i^g = 1$, its expression may vary depending on the user. With the constraint (5) in mind, ℓ^L can be uniformly expressed as a function of n_i^* , given by $\ell^L = n_i^* \mathcal{L}_i(1)$. In contrast to ℓ^R and ℓ^L , terms ℓ^T and ℓ^E only exist in the E2E latency for users whose requests are granted. Specifically, for ℓ^T , it consists of the latency for both the uplink transmission of the prompt and the downlink transmission for the intermediate result. We denote the data sizes of the prompt and intermediate noisy data by s_i^p , and s_i^m , respectively. Although JPEG encoding may cause different split points to produce varying levels of image noisiness, which can slightly affect the data size of intermediate results, these differences have a negligible impact on the E2E latency. Therefore, we assume the data size of the intermediate results to be constant. Then, ℓ_i^T for the granted users with $x_i^g = 1$ can be calculated by

$$\ell_i^T = \frac{s_i^p}{\eta W_i^g} + \frac{s_i^m}{\eta W_i^g}, \quad (7)$$

where W_i^g represents the bandwidth allocated to user i . According to the straightforward bandwidth allocation described in Section 3.1, where granted users share the bandwidth equally, we have

$$W_i^g = \frac{W_{\max}}{\sum_{i \in \mathcal{I}} x_i^g}. \quad (8)$$

The calculation of ℓ_i^E shares certain similarity with that of ℓ_i^T . However, calculating the computational latency for edge offloading presents more complications. Due to the varying split points n_i^* for each user, the batch size may change during the offloaded inference process, as shown in Fig. 2, leading to potentially different computational latency

for each denoising step. Nonetheless, considering that the number of denoising steps predominantly influences the overall latency, we simplify the modeling of the batch size's impact on latency. The batch size during the offloading at the edge is assumed to be fixed as

$$b_g = \sum_{i \in \mathcal{I}} x_i^g. \quad (9)$$

This simplification neglects the impact of certain tasks completing early on the reduction of the denoising step latency for the remaining tasks. With the batch size to the maximum value, it provides a conservative estimate of the worst-case latency. In this context, ℓ_i^E can be expressed by

$$\ell_i^E = (N - n_i^*) \mathcal{L}_e(b_g, G). \quad (10)$$

In light of above, since we aim to optimize the overall performance of all the users, the optimization problem of the offloading strategy can be formulated as

$$\max_{\mathbf{x}, \mathbf{n}^*} \sum_{i \in \mathcal{I}} \alpha_i \mathcal{F}(n_i^*) - L_i \quad (\text{P1})$$

subject to

$$(2), (3), (4), (5).$$

Proposition 1. *The multi-dimensional coupled integer programming problem shown in (P1) is NP-hard.*

Proof. As shown in (P1), there are two sets of coupled optimization variables, \mathbf{x} and \mathbf{n}^* with high dimensions of $|\mathcal{I}| \times |\mathcal{D}|$ and $|\mathcal{I}| \times 1$, respectively. To demonstrate that (P1) is an NP-hard problem, we first simplify it into the form of a standard NP-hard problem, ensuring that the fundamental complexity and core structure remain unchanged. Then, based on the transitivity of NP-hardness, we infer that the original problem is also NP-hard. Specifically, we fix the value of the decision variable n_i^* by $n_i^* = \hat{N}$ for the granted users, assuming that these users do not have high demands for image quality and are primarily focused on reducing latency. Once users opt for offloading, they offload the maximum possible number of denoising steps, i.e., $(N - \hat{N})$. In this sense, the PAI metric $\sum_{i \in \mathcal{I}} \alpha_i \mathcal{F}(n_i^*)$ can be reduced to a function dependent solely on \mathbf{x} , i.e.,

$$\sum_{i \in \mathcal{I}} \alpha_i \mathcal{F}(n_i^*) = \sum_{i \in \mathcal{I}} \sum_{j \in \mathcal{D}} C_{ij} x_i^j, \quad (11)$$

where $C_i^d = \alpha_i \mathcal{F}(N)$ and $C_i^g = \alpha_i \mathcal{F}(\hat{N})$. Meanwhile, C3 and C4 are removed. Moreover, for the penalty term related to latency, substituting (8) into (7), we have

$$\ell_i^T = \sum_{i' \in \mathcal{I}} A_{i'gig}^T \cdot x_{i'}^g \cdot x_i^g, \quad (12)$$

where $A_{i'gig}^T = \frac{s_i^p + s_i^m}{\eta W_{\max}}$. Considering the overall transmission latency of the multi-user system, we have

$$L^T = \sum_{j \in \mathcal{D}} \sum_{j' \in \mathcal{D}} \sum_{i \in \mathcal{I}} \sum_{i' \in \mathcal{I}} A_{i'j'ij}^T \cdot x_{i'}^{j'} \cdot x_i^j, \quad (13)$$

where $A_{i'j'ij}^T = 0$, if $j = d$ or $j' = d$. Similarly, substituting (9) into (10), and explicitly expanding the form of the

function $\mathcal{L}_e(b, G) = k_e(b/G) + h_e$, we have

$$\ell_i^E = D_{ig}^E \cdot x_i^g + \sum_{i' \in \mathcal{I}} A_{i'gig}^E \cdot x_{i'}^g \cdot x_i^g, \quad (14)$$

where $D_{ig}^E = (N - \hat{N})h_e$ and $A_{i'gig}^E = (N - \hat{N})k_e/G$. When extending to multi-user system, we have

$$L^E = \sum_{i \in \mathcal{I}} \sum_{j \in \mathcal{D}} D_{ij}^E \cdot x_i^j + \sum_{j \in \mathcal{D}} \sum_{j' \in \mathcal{D}} \sum_{i \in \mathcal{I}} \sum_{i' \in \mathcal{I}} A_{i'j'ij}^E \cdot x_{i'}^{j'} \cdot x_i^j, \quad (15)$$

where $D_{id}^E = 0$ and $A_{i'j'ij}^E = 0$, except for $A_{i'gig}^E$. In addition, for the latency for local inference, similarly, we have

$$L^L = \sum_{j \in \mathcal{D}} \sum_{i \in \mathcal{I}} D_{ij}^L \cdot x_i^j, \quad (16)$$

where $D_{id}^L = N(k_i + h_i)$ and $D_{ig}^L = \hat{N}(k_i + h_i)$. At last, for L^R , we have

$$L^R = \sum_{j \in \mathcal{D}} \sum_{i \in \mathcal{I}} D_{ij}^R \cdot x_i^j, \quad (17)$$

where $D_{ij}^R = K - k_i$, and k_i denotes the moment when user i sends the request to the edge, as stated in Section 3.1.

Overall, with (11), (13), (15), (16), and (17), the objective function of (P1) can be rewritten as

$$\max_{\mathbf{x}} \sum_{i \in \mathcal{I}} \sum_{j \in \mathcal{J}} D_{ij} \cdot x_i^j - \sum_{j \in \mathcal{D}} \sum_{j' \in \mathcal{D}} \sum_{i \in \mathcal{I}} \sum_{i' \in \mathcal{I}} A_{i'j'ij} \cdot x_{i'}^{j'} \cdot x_i^j, \quad (18)$$

where $D_{ij} = C_{ij} - (D_{ij}^L + D_{ij}^E + D_{ij}^R)$ and $A_{i'j'ij} = A_{i'j'ij}^T + A_{i'j'ij}^E$. According to [31, Theorem 1], the linear term can be removed from (18) as the diagonal of matrix of quadratic terms. Then, (18) can be reformulated as

$$\max_{\mathbf{x}} \sum_{j \in \mathcal{D}} \sum_{j' \in \mathcal{D}} \sum_{i \in \mathcal{I}} \sum_{i' \in \mathcal{I}} \tilde{A}_{i'j'ij} \cdot x_{i'}^{j'} \cdot x_i^j, \quad (19)$$

where $\tilde{A}_{ijij} = D_{ij} - A_{ijij}$ while all other elements of $\tilde{A}_{i'j'ij} = -A_{i'j'ij}$, $i' \neq i, j' \neq j$ remain unchanged. If $|\mathcal{D}| = |\mathcal{I}|$, the optimization problem in (19) is a QAP. However, in the vast majority of cases, $|\mathcal{D}| \ll |\mathcal{I}|$. Additionally, considering the remaining constraint C2 in (3) from the original problem (P1), the simplified version can be more accurately described as a GQAP, widely proven to be NP-hard [32], [33]. Since the reduced problem (19) remains NP-hard, the original (P1) includes additional constraints and variables, making it more complex, it is reasonable to infer that (P1) is at least NP-hard. \square

5 DRL-CONVEX HYBRID SOLUTION FOR EFFICIENT EDGE-ASSISTED OFFLOADING

To address one of the most challenging COPs, the GQAP, further complicated by the additional optimization of a coupled decision variable of integer index vector, in this section, we propose a novel DRL-convex hybrid approach, as shown in Fig. 5. In preparation for algorithmic development, we first transform the extended GQAP with two coupled decision variables \mathbf{x} and \mathbf{n}^* into two nested sub-problems with \mathbf{x} and \mathbf{n}^* , respectively, which is detailed in Section 5.1.

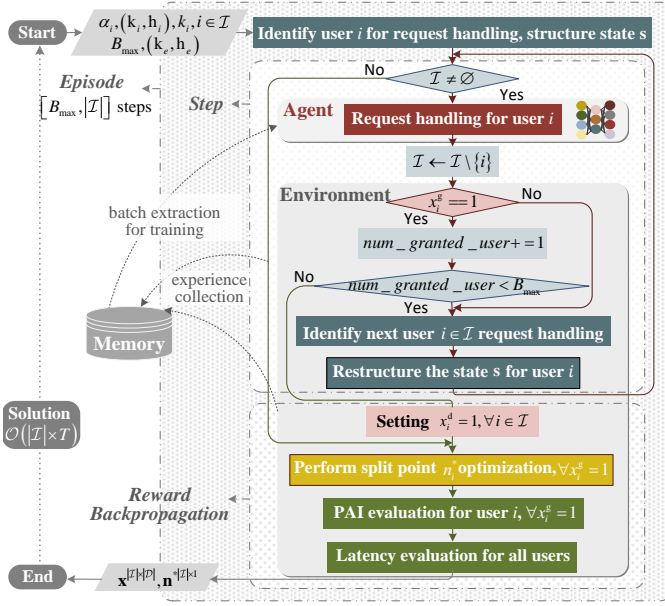


Fig. 5: Flowchart for transitioning from extended GQAP to decision sequence.

5.1 Nested Sub-Problem Formulation

Recall the original problem (P1): the optimal values of \mathbf{x} and \mathbf{n}^* are interdependent. Specifically, the total number of granted users identified by \mathbf{x} determines the latency for each offloaded denoising step at the edge server by setting the batch size during inference. This, in turn, influences the trade-off between PAI and E2E latency by varying degrees for users with diverse computational capacities (k_i, h_i) and emphasis factors α_i , thereby affecting the optimal value of n_i^* . Meanwhile, the value of n_i^* for each user i determines their local inference latency ℓ_i^L , and offloaded inference latency ℓ_i^E , respectively, thereby influencing the optimal choice of \mathbf{x} to minimize the overall E2E latency.

Nevertheless, through an in-depth analysis of the nature of the coupling, variable \mathbf{x} of the two acts as a dominant decision variable. Once the value of \mathbf{x} is set, the optimal value of n_i^* for the individual user i can be solved separately with relative ease. However, \mathbf{n}^* cannot be pre-set to readily determine \mathbf{x} , creating an asymmetric dependency. With this in mind, we transform the original problem into two nested sub-problems. Specifically, we treat the split point optimization problem about individual n_i^* as the *inner* sub-problem, which is solved first based on a feasible solution of \mathbf{x} . Given the *explicit and concrete formulation* of the problem and the general expression across all users, we employ *convex* optimization to solve it with continuous relaxation. Then, the solution of \mathbf{n}^* informs the outer sub-problem about \mathbf{x} to proceed the outer optimization. Due to the *high dimensionality* of decision variable \mathbf{x} in the outer sub-problem, combined with the *complex relationship* between \mathbf{x} and the optimization objective, we adopt a DRL-based approach to effectively solve this problem. *Meanwhile, the implicit dependency of the optimal \mathbf{x} on the informed \mathbf{n}^* , stemming from (P1), can be incorporated into the environment modeling in DRL paradigm.* This approach helps prevent any negative impact of the nested sub-problem formulation on the optimality of

(P1). Next, we detail the solutions to the inner sub-problem, *split point optimization*, and the outer sub-problem, *request handling optimization* in Sections 5.2 and 5.3, respectively.

5.2 Convex Optimization for Split Point Selection

In this subsection, we first analyze the convexity of the optimization problem, followed by specifying the method for determining the optimal solution. Finally, based on the problem analysis, we provide insights on selecting emphasis values for users with varying computational capacities.

For the users with $x_i^d = 1$, we set $n_i^* = N$ directly. Moreover, we have that $L_i = \ell_i^R + \ell_i^L$, which is solely determined by the moment when the user sends request and the computing power of the local device. In this sense, given a feasible \mathbf{x} , the inner optimization problem on the split point only needs to perform for user i with $x_i^s = 1$. Moreover, for the granted users, ℓ_i^T is only dependent on \mathbf{x} , which can be seen as a constant for a given \mathbf{x} . Meanwhile, the value of ℓ_i^E , which should be joint determined by \mathbf{x} and n_i^* , is only dependent in n_i^* for a given \mathbf{x} . Therefore, to ensure clarity in the subsequent analysis, we simply $\ell_i^E(n_i^*, \mathbf{x})$ and $\ell_i^T(\mathbf{x})$ to $\ell_i^E(n_i^*)$ and ℓ_i^T , respectively. In this context, the inner sub-problem can be specifically formulated as follows:

$$\max_{n_i^* \in [\hat{N}, N]} \alpha_i \mathcal{F}(n_i^*) - (\ell_i^R + \ell_i^E(n_i^*) + \ell_i^T + \ell_i^L(n_i^*)). \quad (\text{P2})$$

Proposition 2. *The split point n_i^* optimization is concave problem with a unique optimal solution within the domain $[\hat{N}, N]$.*

Proof. For simplicity, we combine the constant terms that are independent of n_i^* . Recall that $\ell_i^E = (N - n_i^*)\mathcal{L}_e(b_g, G)$ and $\ell_i^L = n_i^*\mathcal{L}_i(1)$, the objective function is rewritten as

$$\mathcal{O}(n_i^*) = \alpha_i \mathcal{F}(n_i^*) - (\mathcal{L}_i(1) - \mathcal{L}_e(b_g, G))n_i^* + \Gamma, \quad (20)$$

where $\Gamma = \ell_i^R + \ell_i^T - N\mathcal{L}_e(b_g, G)$. Recall the expression of $\mathcal{F}(n_i^*) = \frac{1}{1 + \exp(-a_{\mathcal{F}}(x - b_{\mathcal{F}}))}$ as well as the second derivative of the sigmoid function, we have

$$\frac{d\mathcal{O}(n_i^*)}{dn_i^*} = \alpha_i a_{\mathcal{F}} \mathcal{F}(n_i^*) (1 - \mathcal{F}(n_i^*)) - (\mathcal{L}_i(1) - \mathcal{L}_e(b_g, G)),$$

$$\frac{d^2\mathcal{O}(n_i^*)}{d(n_i^*)^2} = \alpha_i a_{\mathcal{F}}^2 \mathcal{F}(n_i^*) (1 - \mathcal{F}(n_i^*)) (1 - 2\mathcal{F}(n_i^*)).$$

Considering that both α_i and $a_{\mathcal{F}}$ are positive and $\mathcal{F}(n_i^*) \in (0, 1)$, the sign of $\frac{d^2\mathcal{O}(n_i^*)}{d(n_i^*)^2}$ depends on $(1 - 2\mathcal{F}(n_i^*))$. As shown in Fig. 4(b), when $n_i^* \in [\hat{N}, N]$ as shown in Fig. 4(b), $\mathcal{F}(n_i^*) > 0.5$. Therefore, $\frac{d^2\mathcal{O}(n_i^*)}{d(n_i^*)^2}$ is constantly less than 0 within the domain. In this sense, $\mathcal{O}(n_i^*)$ is strictly concave. Within $[\hat{N}, N]$, (P2) has a unique optimal solution.

Firstly, in case of $\mathcal{L}_i(1) < \mathcal{L}_e(b_g, G)$, which means that the local inference latency per denoising step is lower than the inference latency at the edge server, $\frac{d\mathcal{O}(n_i^*)}{dn_i^*}$ is strictly positive. In this context, when $n_i^* = N$, (P2) reaches its maximum value, which implies that user i completes inference locally. In contrast, if $\mathcal{L}_i(1) > \mathcal{L}_e(b_g, G)$, the solution has three possible cases. Given that $\frac{d^2\mathcal{O}(n_i^*)}{d(n_i^*)^2} < 0$, $\mathcal{O}'(n_i^*) = \frac{d\mathcal{O}(n_i^*)}{dn_i^*}$ is monotonically decreasing on $[\hat{N}, N]$. Denote the term of $\alpha_i a_{\mathcal{F}} \mathcal{F}(n_i^*) (1 - \mathcal{F}(n_i^*))$ by $\bar{\mathcal{F}}'(n_i^*)$.

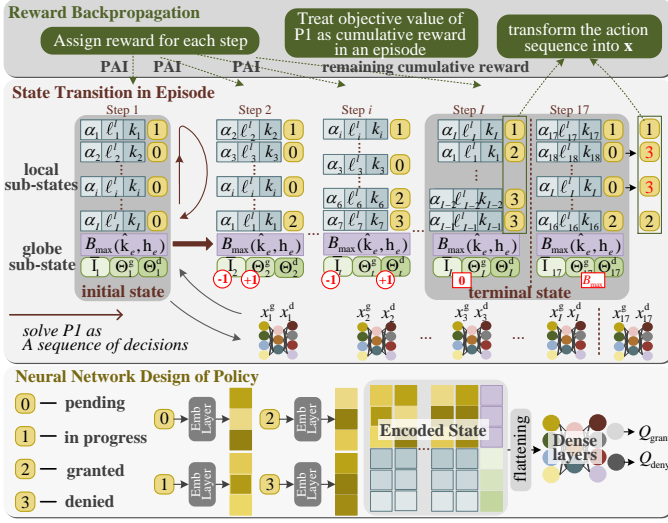


Fig. 6: Illustration of DQN-based request handling.

If $\bar{\mathcal{F}}'(\hat{N}) > \bar{\mathcal{F}}'(N) > (\mathcal{L}_i(1) - \mathcal{L}_e(b_g, G))$, $\mathcal{O}(n_i^*)$ is monotonically increasing within the domain, and $n_i^* = N$. If $\bar{\mathcal{F}}'(N) < \bar{\mathcal{F}}'(\hat{N}) < (\mathcal{L}_i(1) - \mathcal{L}_e(b_g, G))$, $\mathcal{O}(n_i^*)$ is monotonically decreasing within the domain, and $n_i^* = \hat{N}$. In contrast, in case of $\bar{\mathcal{F}}'(N) < (\mathcal{L}_i(1) - \mathcal{L}_e(b_g, G)) < \bar{\mathcal{F}}'(\hat{N})$, there exists a value of n_i^* that makes $\frac{d\mathcal{O}(n_i^*)}{dn_i^*} = 0$, which is the optimal solution. Due to the difficulty in obtaining a closed-form expression for n_i^* , its solution can be found using libraries for solving equations, such as SciPy. \square

Remark 1. In the optimal solution analysis above, for users whose local inference speed is lower than the inference speed of edge offloading, the value of α_i can be determined based on the following guidelines. For a given $\alpha_i > \frac{(\mathcal{L}_i(1) - \mathcal{L}_e(b_g, G))}{a_{\mathcal{F}} \bar{\mathcal{F}}(N)(1 - \bar{\mathcal{F}}(N))}$, the focus of user i on PAI is overwhelmingly dominant. For a given $\alpha_i < \frac{(\mathcal{L}_i(1) - \mathcal{L}_e(b_g, G))}{a_{\mathcal{F}} \bar{\mathcal{F}}(N)(1 - \bar{\mathcal{F}}(N))}$, the optimization problem effectively reduces to optimizing solely for latency. In contrast, for $\frac{(\mathcal{L}_i(1) - \mathcal{L}_e(b_g, G))}{a_{\mathcal{F}} \bar{\mathcal{F}}(N)(1 - \bar{\mathcal{F}}(N))} < \alpha_i < \frac{(\mathcal{L}_i(1) - \mathcal{L}_e(b_g, G))}{a_{\mathcal{F}} \bar{\mathcal{F}}(N)(1 - \bar{\mathcal{F}}(N))}$, it can achieve a personalized trade-off between PAI and latency, with larger values of α_i placing greater emphasis on PAI. Although the exact value of b_g is unknown, the service provider can estimate \hat{b}_g based on the number of active users in the area, thereby offering each user a range for selecting α_i . Additionally, it should be noted that the latency optimization considered in the individual split point only accounts for the computational latency. To incorporate other types of latency integrated in Γ , the exponent of the total latency term in $\mathcal{O}(n_i^*)$ can be increased accordingly.

5.3 DRL-based Request Handling Optimization

In this subsection, we aim to present a novel low-complexity DRL-based algorithm for the outer problem of an extended GQAP. Specifically, to solve the problem using DRL, we first formulate it as a sequential decision problem, which is detailed in Section 5.3.1. Subsequently, the optimal decision variable \mathbf{x} is determined by progressively making step-by-step decisions that optimize the long-term reward, corresponding to the objective of (P1). The decision-making policy for each step is introduced in Section 5.3.2.

5.3.1 MDP construction

We choose a sequential formulation as shown in Fig. 5, where each user's request handling performed by an agent is treated as a single step. Meanwhile, an entire episode ends once the handling results of all users' requests are derived. The specific MDP is described as below.

State Space: To facilitate the agent to provide the optimal solution for a specific scenario, it is essential to incorporate all factors related to the objective value into the state. This includes both *static* information about all users and the edge server, such as computing power, and *dynamic* information shaped by decisions in prior steps. Specifically, as shown in Fig. 6, we define the state as comprising both local and global sub-states, each further divided into static and dynamic elements. Denote the index of steps by t . The local sub-state for user i is denoted by $\mathbf{s}_{t,i}^l = [\alpha_i, l_i, k_i; o_{i,t}]$. Therein, α_i is the emphasis of user i on the PAI and E2E latency, k_i is the moments when user i sends the request to user i , and $l_i = k_i + h_i$ represents the latency per local denoising step, which is dependent on the computing power of user i 's device. These three elements are static during the environment evolution. In contrast, $o_{i,t}$ is the dynamic element, which acts as the indicator of four status. For users whose requests are not handled, $o_{i,t} = 0$; for the user which is identified to be in progress of request handling in the current step, $o_{i,t} = 1$; for the user whose request has been granted, $o_{i,t} = 2$; and for the users whose request has been denied, $o_{i,t} = 3$. For clarity, we denote the index of the user with $o_{i,t} = 1$ as $i = t$. Meanwhile, the globe state is denoted by $\mathbf{s}_t^g = [B_{\max}, \hat{k}_e, h_e; \bar{I}_t, \Theta_t^g, \Theta_t^d]$. Similarly, the first three elements are static, where B_{\max} represents the maximum number of users allowed to offload to the edge server in a round, and \hat{k}_e ($\hat{k}_e = k_e/G$), together with h_e jointly characterizes the computing power of the edge server. Meanwhile, \bar{I}_t , Θ_t^g , and Θ_t^d are the dynamic elements in the globe sub-state, which represent the total number of the users in pending, the total number of the granted users, and the total number of the denied users, respectively. In this context, as shown in Fig. 6, the complete representation of the state can be given by $\mathbf{s}_t = [\mathbf{s}_{t,t}^l, \mathbf{s}_{t,t+1}^l, \dots, \mathbf{s}_{t,I}^l, \mathbf{s}_{t,1}^l, \dots, \mathbf{s}_{t,i}^l, \dots, \mathbf{s}_{t,t-1}^l, \mathbf{s}_t^g]$.

Action Space: In each step t , the action of agent is to grant or deny the offloading request of user i from the perspective of optimizing overall system performance. In this context, we have $a_t \in \{0, 1\}$. If $a_t = 1$, $x_t^g = 1$ and $x_t^d = 0$, otherwise, $x_t^d = 1$ and $x_t^g = 0$.

Transition Rule: The state transition is determined solely by the action in a deterministic manner. Assume that in step t , the request of user t is in progress. Then, in the next state \mathbf{s}_{t+1} , $\bar{I}_{t+1} = \bar{I}_t - 1$. Moreover, if $a_t = 1$, $o_{t,t+1} = 2$ and $\Theta_{t+1}^d = \Theta_t^d + 1$, otherwise $o_{t,t+1} = 3$ and $\Theta_{t+1}^d = \Theta_t^d + 1$. Meanwhile, the indicator of the user for request handling in the next step is set to 1, i.e., $o_{t+1,t+1} = 1$. Moreover, to enable the agent to more easily capture the distinct characteristics of the currently selected user, we apply cyclic shifting as shown in Fig. 6 to consistently position this sub-state at the beginning of the local sub-state. Additionally, there are two conditions for the end of an episode during the transition process: 1) if, in a state, $\bar{I}_t = 0$, it signifies that all users' requests have been processed, then the episode ends 2) if, in a state, the value of $\Theta_t^g = B_{\max}$, it indicates that the

maximum limit of granted users has been reached, then the remaining users' requests are directly considered as denied and the episode ends.

Reward: Due to the batching technique, the total number of granted users b_g affects the inference latency for each offloaded denoising step for each user, which in turn impacts the E2E latency and PAI. Therefore, until the end of an episode, the exact QoE for each user cannot be determined. As shown in Fig. 5, we calculate the cumulative reward function, i.e., the value of the objective function, after the episode ends. Additionally, to mitigate the difficulties that sparse rewards present to the agent's learning, we implement reward backpropagation: the PAI achieved by each user in each step is treated as an immediate reward in each step of the episode, while the difference between the cumulative reward and the cumulative PAI from previous steps serves as the reward for the final step of the episode. The specific formulation is shown as

$$r_t = \begin{cases} \alpha_t \mathcal{F}(n_t^*), & \text{done} = \text{FALSE}, \\ \sum_{i=t}^I \alpha_i \mathcal{F}(n_i^*) - \sum_{i=1}^I L_i, & \text{done} = \text{TRUE}, \end{cases} \quad (21)$$

where I represents the total number of users sending the request for offloading, and the flag "done" serves as an indicator of whether the episode has ended.

5.3.2 PER-DQN-based policy design

Recall (21); the objective function in (P1) is transformed into the expected cumulative reward $\mathbb{E}[\sum_{t \in \mathcal{I}} \gamma^t r_t]$, with $\gamma = 1$. Considering the discrete and small action space, we choose the simple, low-complexity DQN algorithm [34] to learn a policy π to maximize the action-state value at each step, which is defined as $Q(s_t, a_t) \triangleq \mathbb{E}[\sum_{t'=t}^{I_{\text{end}}} \gamma^{t'} r_{t'} | s_t, a_t]$. The optimal action-value function is defined as $Q^*(s_t, a) \triangleq \max_{\pi} Q_{\pi}(s_t, a)$, from which the optimal policy can be decided as $\pi^* = \arg \max_a Q^*(s_t, a)$. Then, the Bellman equation for $Q^*(\cdot)$ can be expressed by

$$Q^*(s_t, a_t) = \mathbb{E} \left[r_t + \gamma \max_a Q^*(s_{t+1}, a) | s_t, a_t, \pi^* \right]. \quad (22)$$

To enable the agent to accurately learn the Q-values corresponding to different (s_t, a_t) , and more easily capture changes in the indicator, we use a neural network (NN) to model the relationship. Specifically, as shown in Fig. 6, we first embed the indicator within each local sub-state and then concatenate it with the static elements. Finally, the encoded state is flattened and fed into the dense layers.

To help the agent find the optimal policy, we utilize a hybrid of ϵ -greedy exploration [34] and Boltzmann exploration [35]. Moreover, in order to keep the learning stability, we use two NNs with the same structure and the initial weights. One named current network is used to choose the action, the weights of which are denoted by θ_c and update in each training step. The other named target network is used to calculate the Q-value, the weights of which are denoted by θ_t and update periodically according to θ_c . In each step, the agent samples a mini-batch of the experiences from the *memory* to train the NN. The loss function used in training is given by

$$\mathcal{L}_{\text{loss}} = \mathbb{E} \left[\left(y_t - \left(\max_a Q^*(s_t, a; \theta_c) \right) \right)^2 \right], \quad (23)$$

where $y_t = r_t + \gamma \max_a Q^*(s_{t+1}, a; \theta_t)$. Moreover, given the high variance in experiences, we assign the experience about the terminal state more attention. When sampling experiences, we set the ratio of selected terminal states to preceding states at 1:7. Meanwhile, we also employ Prioritized Experience Replay (PER) [36], where the experiences are sampled based on their significance, prioritizing transitions with higher learning potential to improve training efficiency. The setting of hyperparameters is detailed in Section 6.

6 SIMULATION AND EVALUATION

6.1 Simulation Setup

6.1.1 Scenario parameter settings

We consider a scenario involving a single edge server and multiple users sending offloading requests within the past Δ . In the following simulations, the determination of inference delay and PAI is based on empirical functions derived from actual experiments, as shown in Figs. 3 and 4 in Section 3. Specifically, we assume that the edge server is equipped with G GPUs, all of the H100 NVL, while users have a single, varying local GPU, which could be one of the other types: {RTX 2060, GTX 1080, ..., RTX 4090}. Meanwhile, the emphasis α_i of user i on the PAI and the latency is randomly selected from the interval $\left[\frac{\mathcal{L}_i(1) - \mathcal{L}_e(\hat{b}_g, G)}{a_{\mathcal{F}} \mathcal{F}(\hat{N})(1 - \mathcal{F}(\hat{N}))}, \frac{\kappa(\mathcal{L}_i(1) - \mathcal{L}_e(\hat{b}_g, G))}{a_{\mathcal{F}} \mathcal{F}(\hat{N})(1 - \mathcal{F}(\hat{N}))} \right]$, where we set $\hat{b}_g = 20$ and $\kappa = 0.05$. The introduction of κ accounts for the fact that users sending offloading requests tend to be more sensitive to latency to varying extend. Moreover, we set the total bandwidth $W_{\text{max}} = 1$ MHz. Assuming the base station employs power control, the spectral efficiency for each user is set as $\eta = 10$ bits/s/Hz. Considering that the data sizes of the intermediate noisy image and prompt of different users are approximately equal, we substitute the specific noisy image and prompt for each user with their respective means. Thus, we have $s_i^p = 216$ b, and $s_i^m = 4.4$ Mb.

6.1.2 PER-DQN hyperparameter settings

The Q-network consists of one embedding layer, three hidden linear layers and an output layer. The vocabulary size and embedding dimension of the embedding layer are set as 4 and 3, respectively. Each of the hidden linear layer has 256 nodes. The output layer has two nodes. The target network is updated at a frequency of once every 2000 time steps. The memory capacity is 400000, the batch size is 128, and the learning rate is 0.0001. The exploration probability ϵ linearly decreases from 0.5 to 0.001. The temperature parameter of Boltzmann exploration linearly decreases from 5 to 0.01. During PER, the priority exponent is set to 0.7, the importance sampling weight is set to 0.3, and the priority offset is set to 0.00002. Moreover, during training, the reward is scaled to 0.1 of its original value.

6.2 Performance Analysis

Firstly, we analyze the key factors influencing the optimal offloaded denoising steps and their respective impacts. As shown in Fig. 7a, given an edge server with 8 available GPUs, as the batch size at the edge increases, the inference latency per denoising step at the edge server lengthens, and

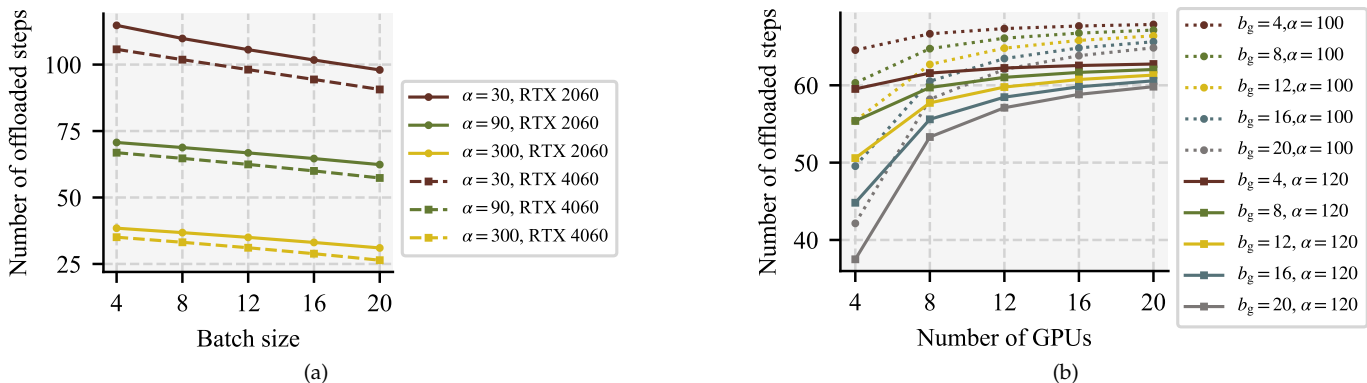


Fig. 7: The relationship between the number of denoising steps offloaded and user emphasis α_i under varying configurations. (a) Analysis with differing batch sizes at the edge server and varying computational capacities of the local terminal. (b) Impact of different numbers of available GPUs on the edge server combined with varying batch sizes.

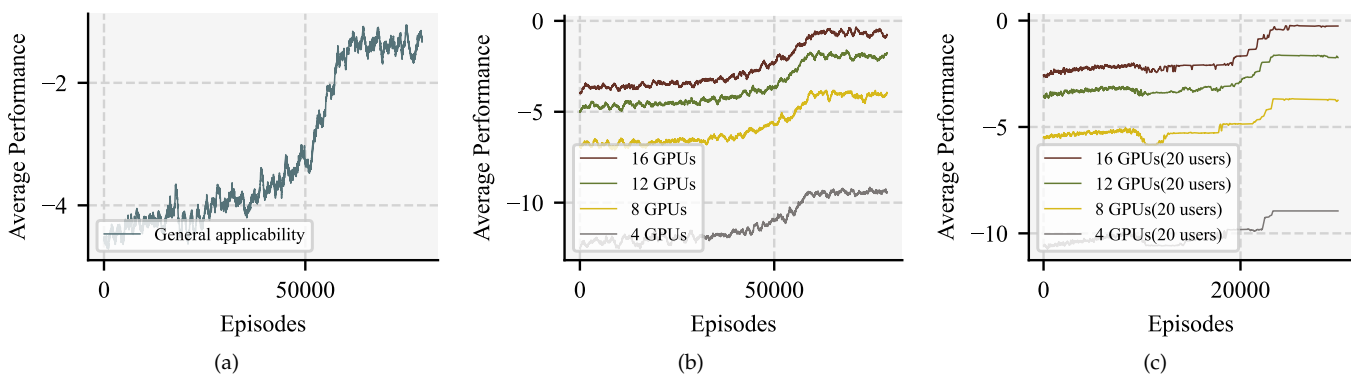


Fig. 8: Learning curves for DRL algorithms with different applicability scopes. (a) General application, where training involves 2000 randomly generated seeds for initialization, with curves smoothed using a moving average window of 1000. (b) GPU-constrained application, where training involves 1000 randomly generated seeds for environment initialization, with curves smoothed using a moving average window of 1000. (c) Specific application, where training involves a single random seed for environment initialization, with curves smoothed using a moving average window of 100.

the optimal number of offloaded steps gradually decreases. Additionally, for the same batch size, the stronger the computational capacity of the user’s local device, the fewer offloaded steps are required, with more denoising steps executed locally. Furthermore, as illustrated in Fig. 7b, with an increase in the number of GPUs on the edge server and the resulting improvement in inference speed, the optimal number of offloaded steps also increases. Both sub-figures indicate that as the value of α_i increases, reflecting heightened user focus on PAI, the optimal offloaded steps decrease accordingly. Moreover, when computational resources are relatively abundant, α_i exerts a dominant influence on the optimal offloading steps. Conversely, with a smaller number of available GPUs, batch size has a more significant impact on the optimal number of offloaded steps.

Next, we integrate the aforementioned split point optimization into the modeling of environmental transitions in the MDP model. Through simulations, we verify the effectiveness of the proposed DQN-convex hybrid solution. Given different applicability scopes, we train three types of Q-networks tailored for the following three scenarios:

- *General Applicability*: For scenarios with evolving com-

putational resources at the edge, dynamic numbers of users, and various user combinations, with a greater emphasis on the algorithm’s generalizability.

- *GPU-Constrained Applicability*: For cases with specific computational resources, dynamic numbers of users, and various user combinations, striking a balance between generalizability and optimality.
- *Specific Applicability*: For scenarios with fixed computational resources, a specific number of users, and a particular user combination, focusing more the with a greater focus on the algorithm’s optimality.

The learning curves for the three application scopes are shown in Fig. 8. From the figure, we can observe that the agent can learn effectively in all three cases. Additionally, the more generalizable the model, the greater the fluctuation in its convergence curve, which is mainly due to the inherent diversity of the environment. Moreover, the performance of models with different applicability scopes is shown in Fig. 9. From Fig. 9a, we observe that the model tailored to specific applications achieves generally superior performance, although the trend remains consistent. Specifically, excluding the impact of local computational heterogeneity

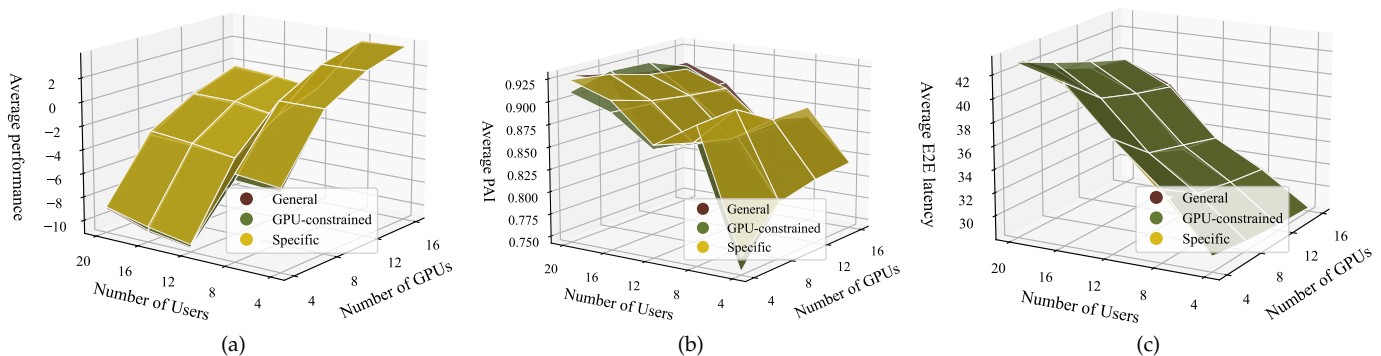


Fig. 9: Performance comparison of three DRL algorithms with different applicability scopes for the same specific case. (a) Overall all performance. (b) Average PAI. (c) Average E2E latency.

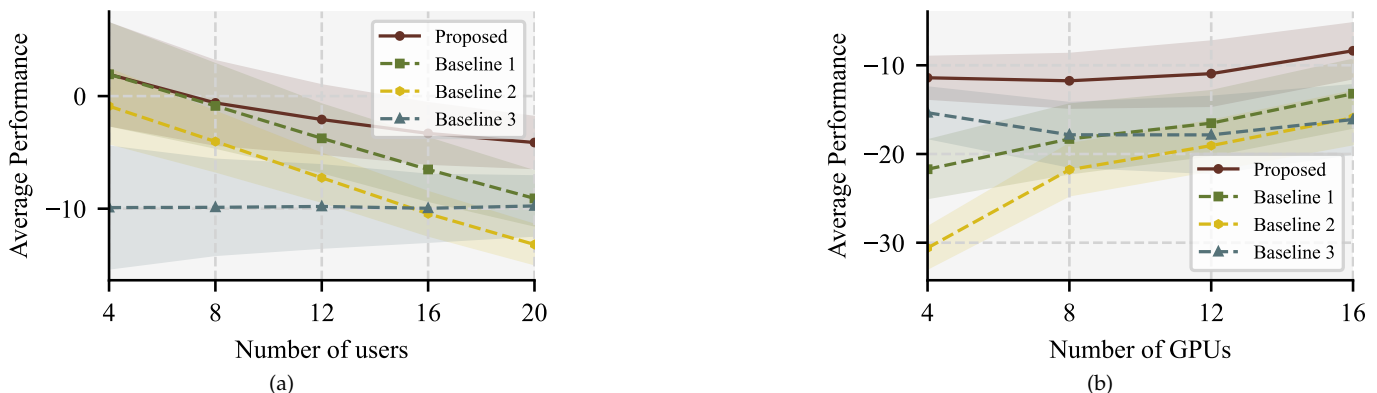


Fig. 10: Performance comparison between the proposed offloading strategy and three baselines: (a) The relationship between overall performance and the number of users, with 100 randomly generated cases for each user count; (b) The relationship between overall performance and the number of available GPUs at the edge server, with 100 randomly generated cases for each GPU configuration.

and user preferences, the average performance tends to increase as the number of users decreases and the number of available GPUs on the edge server increase. As shown in Fig. 9b and 9c, this improvement is primarily due to the inference latency reduction achieved through offloading, which outweighs the performance loss from potential PAI degradation. Given the slight performance difference across the three algorithms, the model for general application is preferred in highly dynamic environments, as it avoids the computational cost associated with frequent retraining and fine-tuning. For scenarios with a fixed set of requesting users, the model tailored for specific applications can be selected to achieve optimal performance. The model for GPU-constrained applications strikes a balance between generality and optimality by training separate models tailored to each GPU availability scenario, leveraging the model redundancy to accommodate varying GPU constraints.

In the subsequent algorithm comparisons, we focus on the more common dynamic scenarios and use the *general model* for performance analysis. Firstly, we compare this algorithm with the commonly used straightforward approaches for personalized diffusion model inference. Three baseline methods considered are as follows:

- *Baseline 1*: Within the maximum batch size supported

by the edge server, all users offload to the edge, with optimization of the split point.

- *Baseline 2*: Within the maximum batch size supported by the edge server, all users offload to the edge, with a fixed offloading of \tilde{N} steps.
- *Baseline 3*: All users perform the complete inference locally.

For baseline 1 and baseline 2, if the total number of users sending requests exceeds the maximum batch size supported by the edge server, users who send requests later perform inference locally. Fig. 10 presents a comparison of the proposed algorithm with three baseline methods, illustrating the performance trends as the number of users and the available GPUs on the edge server vary. Specifically, in Fig. 10a, we fix the number of available GPUs on the edge server to 8, while in Fig. 10b, we fix the number of users in each case to 20. Observing both subfigures, baseline 3, where all inference is completed locally by users, shows no noticeable trend in average performance as the number of users or available GPUs changes. In contrast, for the other three methods, average performance declines as the number of users increases or the number of GPUs decreases. Furthermore, since baseline 1 incorporates split point optimization compared to baseline 2, baseline 1 consistently maintains a

TABLE 1: Complexity comparison regarding user count.

Order \uparrow	Name of Method	Complexity
1	DRL-convex hybrid	$O(I)$
2	Heuristic algorithm	$O(2 \cdot P \cdot M \cdot I)$
3	Branch & Bound	$O(2^{2 \times I})$

stable performance gap above baseline 2. Additionally, due to its joint optimization of split point and request handling, the performance variation of the proposed method is narrower than that of baselines 1 and 2, and it consistently outperforms other baseline algorithms. This result further indicates that the algorithm can flexibly adaptively trade off between PAI and latency across different scenarios, achieving optimal overall performance.

Finally, we demonstrate the effectiveness and optimality of the DRL-convex hybrid solution for the extended GQAP by comparing it with two widely used methods for GQAP: a heuristic algorithm and a branch & bound-based Integer Linear Programming (ILP) method. The heuristic algorithm selects is a genetic algorithm with a population size of $P = 100$ and an iteration count of $M = 200$. Additionally, as the optimal split point lacks a closed-form solution, we omit the split point optimization in the Branch & Bound-based ILP method for simplicity. As illustrated in Fig. 11, the proposed DRL-convex hybrid solution outperforms the other methods, achieving superior performance. Specifically, due to the omit of the split point optimization, the Branch & Bound based method, the optimality of the method consistently remains lower than that of our proposed method. Additionally, although the heuristic algorithm does not require the rigorous mathematical formulation demanded by the Branch & Bound based method, it can incorporate split point optimization. However, its stability in terms of optimality is noticeably lower than that of the other two algorithms. As a result, while it may occasionally achieve the same level of optimality as our proposed DRL-convex hybrid method, its average performance is the poorest. Moreover, the complexity of the three methods with respect to user count I as shown in Table 1. From the table, since in the process of constructing the MDP model, we transform the original problem with high-dimensional optimization variables into a decision sequence problem focused on a single variable, the proposed DRL-convex hybrid method shows a linear complexity of $O(I)$. This linear growth suggests that the DRL-Convex Hybrid Method is scalable and well-suited for scenarios with a large number of users. In contrast, the Heuristic Algorithm-Based Method has a complexity of $O(2 \cdot P \cdot M \cdot I)$. Although it also scales linearly with I , its overall complexity is influenced by P and M , requiring careful parameter tuning to ensure efficiency as the user count rises. In addition, the conventional Branch & Bound-Based Method presents an exponential complexity of $O(2^{2 \times I})$, which grows rapidly with increasing I . This exponential growth makes it work for small-scale problems and impractical for large-scale scenarios, as the computational cost becomes prohibitive. Overall, with a well-trained Q network, the DRL-convex hybrid algorithm is more viable for larger user counts due to their manageable complexity.

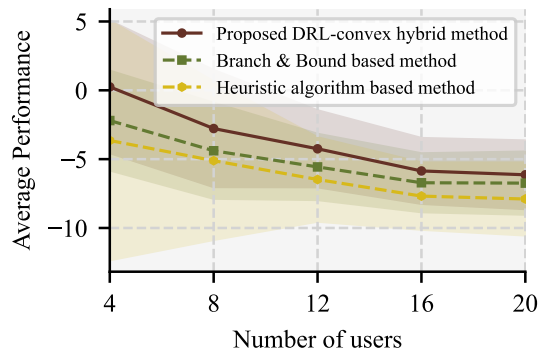


Fig. 11: Performance comparison among proposed DRL-convex hybrid method, Branch & Bound based method, and Heuristic algorithm based method, with 100 randomly generated cases for each user count.

7 CONCLUSION

In this work, we have focused on the practical implementation of personalized diffusion models in multi-user scenarios with diverse local computing capabilities. We have proposed a novel framework for efficient multi-user offloading of personalized diffusion models for a cluster where the users enjoy similar types of personalized generative applications. In this framework, a cluster-wide SDM, trained to capture common personalized demands across users within the cluster, has been deployed at the edge server, while each user's personalized model has been deployed locally. To address the balance between latency and accuracy, we have introduced a customized metric that links these factors via a weighting parameter, providing a parameter range and insights into the trade-offs it entails. We have formulated the joint optimization of offloading request handling and individual user split points as an extended GQAP, aiming to maximize overall performance based on the proposed metric. To meet real-time decision-making requirements, we have applied DRL to tackle GQAP, proposing a DRL-convex hybrid solution—a novel approach. Finally, we have demonstrated the optimality and low complexity of our algorithm through comparisons with classical QAP-solving methods, such as Branch & Bound and heuristic algorithms, showcasing its efficiency and effectiveness.

In future work, we will pursue further optimization from the two perspectives: 1) to enhance the generalization capability of the model, we will design training optimization methods for cluster-specific models, achieving a trade-off between model size and PCI performance; 2) we will explore optimal clustering methods based on task similarity to balance the storage and computational energy consumption of multi-cluster-wide models with PCI performance.

REFERENCES

- [1] R. Rombach, A. Blattmann, D. Lorenz, P. Esser, and B. Ommer, "High-resolution image synthesis with latent diffusion models," in *Proceedings of the IEEE/CVF conference on computer vision and pattern recognition*, 2022, pp. 10 684–10 695.
- [2] J. Ho, A. Jain, and P. Abbeel, "Denosing diffusion probabilistic models," *Advances in neural information processing systems*, vol. 33, pp. 6840–6851, 2020.

- [3] F.-A. Croitoru, V. Hondru, R. T. Ionescu, and M. Shah, "Diffusion models in vision: A survey," *IEEE Transactions on Pattern Analysis and Machine Intelligence*, vol. 45, no. 9, pp. 10 850–10 869, 2023.
- [4] W. Yang, Z. Xiong, S. Mao, T. Q. Quek, P. Zhang, M. Debbah, and R. Tafazolli, "Rethinking generative semantic communication for multi-user systems with multi-modal llm," *arXiv preprint arXiv:2408.08765*, 2024.
- [5] X. Zhang, X.-Y. Wei, W. Zhang, J. Wu, Z. Zhang, Z. Lei, and Q. Li, "A survey on personalized content synthesis with diffusion models," *arXiv preprint arXiv:2405.05538*, 2024.
- [6] J. Song, C. Meng, and S. Ermon, "Denoising diffusion implicit models," *International Conference on Learning Representations*, 2021.
- [7] X. Yang, D. Zhou, J. Feng, and X. Wang, "Diffusion probabilistic model made slim," in *Proceedings of the IEEE/CVF Conference on computer vision and pattern recognition*, 2023, pp. 22 552–22 562.
- [8] G. Fang, X. Ma, and X. Wang, "Structural pruning for diffusion models," in *Advances in Neural Information Processing Systems*, 2023.
- [9] X. Li, Y. Liu, L. Lian, H. Yang, Z. Dong, D. Kang, S. Zhang, and K. Keutzer, "Q-diffusion: Quantizing diffusion models," in *Proceedings of the IEEE/CVF International Conference on Computer Vision (ICCV)*, October 2023, pp. 17 535–17 545.
- [10] E. Liu, X. Ning, Z. Lin, H. Yang, and Y. Wang, "OMS-DPM: Optimizing the model schedule for diffusion probabilistic models," in *Proceedings of the 40th International Conference on Machine Learning*. PMLR, 2023, pp. 21 915–21 936.
- [11] H. Du, R. Zhang, D. Niyato, J. Kang, Z. Xiong, D. I. Kim, X. Shen, and H. V. Poor, "Exploring collaborative distributed diffusion-based ai-generated content (aigc) in wireless networks," *IEEE Network*, vol. 38, no. 3, pp. 178–186, 2024.
- [12] C. Yan, S. Liu, H. Liu, X. Peng, X. Wang, F. Chen, L. Fu, and X. Mei, "Hybrid sd: Edge-cloud collaborative inference for stable diffusion models," *arXiv preprint arXiv:2408.06646*, 2024.
- [13] Y. Balaji, S. Nah, X. Huang, A. Vahdat, J. Song, Q. Zhang, K. Kreis, M. Aittala, T. Aila, S. Laine *et al.*, "ediff-i: Text-to-image diffusion models with an ensemble of expert denoisers," *arXiv preprint arXiv:2211.01324*, 2022.
- [14] E. Liu, X. Ning, Z. Lin, H. Yang, and Y. Wang, "OMS-DPM: Optimizing the model schedule for diffusion probabilistic models," in *Proceedings of the 40th International Conference on Machine Learning*, ser. Proceedings of Machine Learning Research, A. Krause, E. Brunskill, K. Cho, B. Engelhardt, S. Sabato, and J. Scarlett, Eds., vol. 202. PMLR, 23–29 Jul 2023, pp. 21 915–21 936. [Online]. Available: <https://proceedings.mlr.press/v202/liu23ab.html>
- [15] S. Yang, Y. Chen, L. Wang, S. Liu, and Y.-C. Chen, "Denoising diffusion step-aware models," in *The Twelfth International Conference on Learning Representations (ICLR)*, 2024. [Online]. Available: <https://openreview.net/forum?id=c43FGk8Pcg>
- [16] H. Du, R. Zhang, D. Niyato, J. Kang, Z. Xiong, D. I. Kim, X. S. Shen, and H. V. Poor, "Exploring collaborative distributed diffusion-based ai-generated content (aigc) in wireless networks," *IEEE Network*, 2023.
- [17] G. Xie, Z. Xiong, X. Zhang, R. Xie, S. Guo, M. Guizani, and H. V. Poor, "Gai-iov: Bridging generative ai and vehicular networks for ubiquitous edge intelligence," *IEEE Transactions on Wireless Communications*, 2024.
- [18] Q. Cai, Y. Zhou, L. Liu, Y. Qi, and J. Shi, "Prioritized assignment with task dependency in collaborative mobile edge computing," *IEEE Transactions on Mobile Computing*, vol. 23, no. 12, pp. 13 505–13 521, 2024.
- [19] Z. Liu, Q. Lan, and K. Huang, "Resource allocation for multiuser edge inference with batching and early exiting," *IEEE Journal on Selected Areas in Communications*, vol. 41, no. 4, pp. 1186–1200, 2023.
- [20] W. Ma and L. Mashayekhy, "Video offloading in mobile edge computing: Dealing with uncertainty," *IEEE Transactions on Mobile Computing*, vol. 23, no. 11, pp. 10 251–10 264, 2024.
- [21] A. Silva, L. C. Coelho, and M. Darvish, "Quadratic assignment problem variants: A survey and an effective parallel memetic iterated tabu search," *European Journal of Operational Research*, vol. 292, no. 3, pp. 1066–1084, 2021.
- [22] F. Glover and E. Woolsey, "Converting the 0-1 polynomial programming problem to a 0-1 linear program," *Operations research*, vol. 22, no. 1, pp. 180–182, 1974.
- [23] H. D. Sherali and W. P. Adams, "Reformulation-linearization techniques for discrete optimization problems," *Handbook of Combinatorial Optimization: Volume 1–3*, pp. 479–532, 1998.
- [24] A. A. Pessoa, P. M. Hahn, M. Guignard, and Y.-R. Zhu, "Algorithms for the generalized quadratic assignment problem combining lagrangean decomposition and the reformulation-linearization technique," *European Journal of Operational Research*, vol. 206, no. 1, pp. 54–63, 2010.
- [25] E. Khalil, H. Dai, Y. Zhang, B. Dilkina, and L. Song, "Learning combinatorial optimization algorithms over graphs," *Advances in neural information processing systems*, vol. 30, 2017.
- [26] Q. Ma, S. Ge, D. He, D. Thaker, and I. Drori, "Combinatorial optimization by graph pointer networks and hierarchical reinforcement learning," in *AAAI Workshop on Deep Learning on Graphs: Methodologies and Applications*, 2020.
- [27] Q. Cappart, T. Moisan, L.-M. Rousseau, I. Prémont-Schwarz, and A. A. Cire, "Combining reinforcement learning and constraint programming for combinatorial optimization," in *Proceedings of the AAAI Conference on Artificial Intelligence*, vol. 35, no. 5, 2021, pp. 3677–3687.
- [28] M. Pashazadeh and K. Wu, "On the difficulty of generalizing reinforcement learning framework for combinatorial optimization," *arXiv preprint arXiv:2108.03713*, 2021.
- [29] P. S. Bagga and A. Delarue, "Solving the quadratic assignment problem using deep reinforcement learning," *arXiv preprint arXiv:2310.01604*, 2023.
- [30] B.-K. Kim, H.-K. Song, T. Castells, and S. Choi, "Bk-sdm: A lightweight, fast, and cheap version of stable diffusion," *arXiv preprint arXiv:2305.15798*, 2023.
- [31] P. L. Hammer and A. A. Rubin, "Some remarks on quadratic programming with 0-1 variables," *Revue française d'informatique et de recherche opérationnelle. Série verte*, vol. 4, no. V3, pp. 67–79, 1970.
- [32] M. L. Fisher, R. Jaikumar, and L. N. Van Wassenhove, "A multiplier adjustment method for the generalized assignment problem," *Management science*, vol. 32, no. 9, pp. 1095–1103, 1986.
- [33] S. Sahni and T. Gonzalez, "P-complete approximation problems," *Journal of the ACM (JACM)*, vol. 23, no. 3, pp. 555–565, 1976.
- [34] V. Mnih, K. Kavukcuoglu, D. Silver, A. A. Rusu, J. Veness, M. G. Bellemare, A. Graves, M. Riedmiller, A. K. Fidjeland, G. Ostrovski *et al.*, "Human-level control through deep reinforcement learning," *nature*, vol. 518, no. 7540, pp. 529–533, 2015.
- [35] N. Cesa-Bianchi, C. Gentile, G. Lugosi, and G. Neu, "Boltzmann exploration done right," *Advances in neural information processing systems*, vol. 30, 2017.
- [36] T. Schaul, "Prioritized experience replay," *arXiv preprint arXiv:1511.05952*, 2015.